

2D Particle-In-Cell (PIC) Computer Model for Antimatter Plasma Simulation

Clementine C.J. Domine,^{*} project performed in collaboration with Daniel Duque

Department of Physics and Astronomy, University of Manchester, Oxford Road, Manchester M13 9PL, UK

May 2020

ABSTRACT

A particle-in-cell (PIC) computer code aiming at simulating the equilibrium conditions for an antiproton and electron plasma confined in a Penning-Malmberg trap was developed in C++. This code is used for the study of the electron/antiproton separation technique performed in the ALPHA experiment at CERN, called the e-kick procedure. Inside the trap, the antiprotons are cooled through collisions with electrons which radiate the energy through cyclotron radiations. Then, by removing the electrons, the cooled antiprotons can recombine with positrons to produce antihydrogen atoms. The PIC code was further developed, establishing appropriate initial conditions and diagnostics to study the e-kick process. The results of the center and side e-kicks are reported and discussed with a focus on finding the minimum temperature of the antiprotons at the end of the procedure. The average kinetic energy in Kelvin of the plasmas was measured to estimate their temperature after the e-kick. It was found that the e-kick leads to the heating of both the electron and antiproton plasmas. The antiprotons' average energy after the e-kick is larger for the side e-kick. For the center e-kick the average kinetic energy increases by less than 10 percent of the initial temperature, whereas for the side e-kick the average kinetic energy increases up to the triple of the initial temperature. For the side e-kick, a fast and strong kick minimises the average kinetic energy of the antiprotons. The electron plasma is heated to high average kinetic energy ranging between 1×10^3 K and 1×10^5 K for both e-kicks regardless of the initial distribution temperature. A smooth and long kick minimises the average kinetic energy of the electrons for both e-kick types. Overall, the central e-kick seems to be more efficient than the side e-kick as the final energy in the trap is minimized.

1 INTRODUCTION

Computer simulations of plasmas have been studied extensively for over 30 years [1]. These models have succeeded in simulating plasma dynamical behaviours with varying degrees of theoretical and experimental accuracy [2; 3; 4]. The performances of the models have improved with the exponential growth of computer technologies. However, the available computational power and storage capacities keep on limiting the accuracy and speed of the models.

Based on previous works [2; 3; 4], a particle-in-cell (PIC) code model for the simulation of the equilibrium conditions for an antiproton and electron plasma confined in a Penning-Malmberg trap was developed in C++. In the code used for this project, the plasma is discretized as a set of macroparticles. The code can load a simple set of macroparticles and then simulate the time evolution of the plasma inside a trap. A finite difference method is used to determine the potential experienced by each macroparticle by solving the Poisson and Laplace equations [5] on a discrete grid. The potential is then used to solve the equation of motion of each particle, giving the dynamical evolution of the plasma. The model takes advantage of the geometrical symmetries and the timescales of interest to represent the plasmas' three-dimensional behaviours in only two dimensions. The validity and accuracy of the different components of the model were investigated using different initial conditions. Further details of the PIC model can be found in the preliminary report by Daniel Duque [6].

During the second semester of 2020, the code was further developed and used to study the electron removal from an antiproton/electron plasma (e-kick procedure) performed in the antihydrogen experiment ALPHA at

* E-mail: clementine.domine@student.manchester.ac.uk

CERN. Inside the experiment, electrons are used to cool the antiprotons through Coulomb collisions, leaving the antiprotons at a suitable temperature for the formation of antihydrogen atoms. The effect of the e-kick procedure on the antiprotons temperature is studied to determine the optimum e-kick that leaves the antiprotons at a minimal temperature. A procedure to obtain an equilibrium distribution that mimics the plasma inside the ALPHA experiment trap was implemented. Different loading procedures such as using an ergodic quiet start loading were explored [7]. Multiple diagnostics were developed to obtain information on the plasmas state throughout the simulation.

This report is divided into three sections. The first section reviews the e-kick procedure used in the ALPHA experiment and the simplifying assumptions used for this study. In the second section, a review of the progress made on the C++ PIC code can be found along with the details of the computer simulation methods. This comprises the method used to find the thermal equilibrium density distribution, the integration method to distribute the macroparticles in the trap, the diagnostics, and the methods implemented to study the e-kick. The final section of the report presents and discusses the results of the e-kick study using the newly developed program. A focus is given on the comparative study of the center versus the side electrode e-kicks.

2 THE ELECTRON REMOVAL (E-KICK) PROCEDURE

Antiprotons with kinetic energy around 5.3 MeV are sent through a degrader foil to the ALPHA's Penning-Malmberg trap from the Antiproton Decelerator [8; 9]. Through collisions with electrons in the degrader, the beam is slowed down to 5 keV allowing the plasma to be trapped. However, the energy distribution of the trapped antiprotons is outside the range of energies for the recombination to form antihydrogen atoms. To cool the antiprotons, a cold electron plasma of approximately 1×10^7 electrons is trapped between the high voltage electrodes before the arrival of the antiprotons. The energy of the antiprotons is then decreased through Coulomb collisions with the cold electron plasma [10; 11]. Eventually, the non-neutral electron/antiproton plasma reaches an equilibrium state, as the electrons radiate the energy taken away from the antiprotons. The electrons are kicked out of the trap as shown in Fig. 1, allowing the cooled antiprotons to later recombine with positrons and produce antihydrogen atoms. One side of the well is removed thanks to a quick voltage pulse, with a rise time of ~ 10 ns. The voltage V is kept high for a period τ of approximately 100 ns allowing the electrons to escape. To limit the loss of antiprotons, an additional voltage pulse is applied to re-establish the trapping well. The efficiency of antihydrogen production is improved by a lower post-e-kick antiproton temperature. The success of an e-kick is determined as a compromise between the low antiproton temperature, the minimization of the number of electrons and the maximization of the number of antiprotons inside the trap [12; 13]. Repeating the procedure multiple times reduces the effect of the plasma heating allowing sympathetic cooling to take place in a waiting potential after each pulse. The time between each e-kick is determined experimentally to limit the heating of the antiprotons. In the ALPHA experiment, the temperature obtained at the end of the e-kick procedure is ~ 500 K. We aim at simulating the e-kick procedure described above.

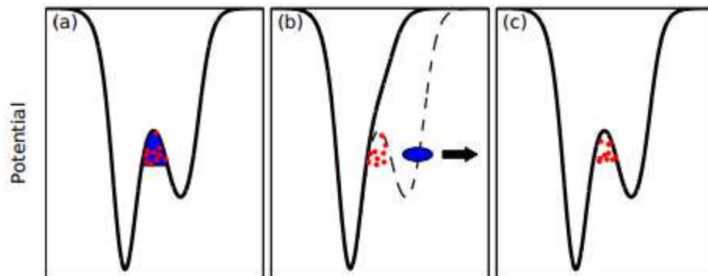


Figure 1. Schematic of the e-kick pulse procedure. The electron-antiproton plasma is initially confined in the e-kick well (a). One side of the high voltage well is raised (b), allowing electrons (blue) to escape. The well is restored (c) before antiprotons (red dots) can escape. Figure taken from [14].

For the purpose of this study, the geometry of the electromagnetic Penning-Malmberg trap is reduced to a set of five identical cylindrical electrodes separated by a gap of 0.5 mm with a length of 13.22 mm and a diameter of 29.76 mm [12; 15]. Each electrode can be set to a chosen voltage to create a trapping potential. The simplified geometry of the Penning-Malmberg trap in the ALPHA experiment is shown in Fig. 2. The reduction of the dimensionality and complexity of the system simplifies the study of the dynamical behaviours of the plasmas [2; 3; 4].

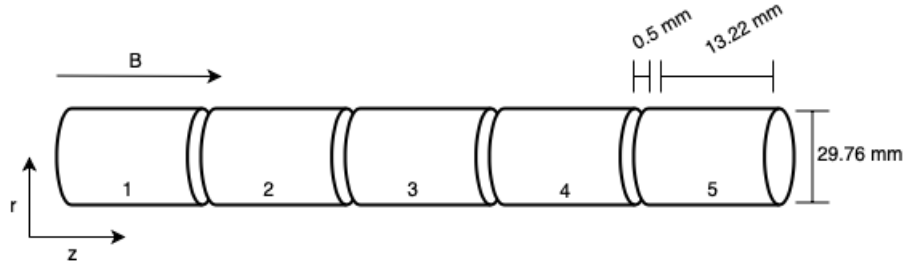


Figure 2. The schematic of the Penning-Malmberg trap similar to the one used in the ALPHA experiment. Five identical electrodes of length 13.22 mm and diameter 29.76 mm separated by a gap of 0.5 mm are represented. A strong magnetic field B is applied along the z direction. The electrodes are numbered 1 through 5.

In this study, the three-dimensional dynamics of the macroparticles are simplified by taking advantage of symmetries and the timescales of interest in accordance with the experimental set up. The plasma loaded inside the Penning-Malmberg trap is assumed to have an azimuthally symmetric initial distribution. Under this hypothesis the plasma dynamics is reduced to a 2-dimensional system. Inside the trap, a large magnetic field is applied to the plasma. Therefore, the radial transport can be neglected as the electron's Larmor radius is negligible compared to any relevant length scale. Moreover, the rotation due to the $\vec{E} \times \vec{B}$ drift is slow compared to the research interest time scale. Finally, the magnetic field contribution emerging from the particle velocity inside the plasma is ignored without loss of accuracy. In consequence, the particles inside the trap move in the axial direction exclusively.

3 COMPUTATIONAL METHOD AND DIAGNOSTICS

This section describes the PIC method implemented for the simulation of the e-kick.

3.1 PIC Code

A detailed description of the C++ PIC code method is given below. The field equation integration is detailed followed by the working order of the simulation.

The plasma is discretized as a set of coupled macroparticles using a mean electric field approximation. The electrostatic potential determines the force experienced by each charged particle in the trap. The total potential is expressed as

$$\phi = \varphi_s + \phi_t, \quad (1)$$

where φ_s and ϕ_t is the self-potential of the plasma emerging from the net charge and the electrostatic potential of the trap, respectively.

The potential ϕ throughout the trap is calculated as follows:

- Laplace's equation is solved to find the electrostatic potential of the trap ϕ_t . The equation is subject to the boundary conditions at the radial edge set by the potential applied to the electrodes. The Neumann boundary conditions [16] are applied at the beginning and the end of the trap as well as at the center of the trap along the radial edge. The electric potential of the trapping well can be obtained by solving Laplace's equation given below

$$\nabla^2 \phi_t = 0, \quad (2)$$

where ϕ_t is the trap potential.

- Poisson's equation is solved to find the self-potential of the plasma φ_s . The equation is subject to Dirichlet boundary conditions of $\varphi_s = 0$ at the electrodes. Additionally, the Neumann boundary conditions are applied at the beginning and the end of the trap as well as at the center of the trap along the radial edge [16]. The self-consistent electric potential can be obtained by solving Poisson's equation given as

$$\nabla^2 \varphi_s = -\frac{\rho}{\epsilon_0}, \quad (3)$$

where ρ is the plasma charge density and ϵ_0 is the permittivity of free space. It is important to note that linear interpolation of the potential is assumed for the gaps between electrodes.

The Laplace and Poisson equations are solved on a two-dimensional grid using a finite difference method [5]. In the region of interest, where the plasma is located, the solvers' accuracy was tested and validated. The grid spans the trap in the radial and axial directions. The dimensionality and geometry of the simulation are justified at the end of section 2. The grid spacing in the radial direction with N_r grid points and axial direction with N_z grid points are estimated with respect to the Debye lengths of the plasmas. The Debye length λ_D gives the characteristic range inside of which the electric effect of a charge gets shielded out by the other charged particles in the plasma. The Debye length is given by the expression [17]

$$\lambda_D = \left(\frac{\epsilon_0 T k_b}{n_0 e^2} \right)^{\frac{1}{2}}, \quad (4)$$

where T is the temperature of the plasma, e is the electric charge of the plasma, n_0 the density of the plasma and k_b is the Boltzmann constant. This parameter is crucial when estimating the number of grid points required to resolve the plasma dynamics. The grid sizes h_z and h_r , along the axial and radial direction respectively, were chosen to resolve the plasmas' Debye length.

The initial charge density is determined by solving the Poisson Boltzmann equation which guarantees the thermal equilibrium of the plasma as explained below in section 3.2.1. The Poisson Boltzmann equation is solved for a total number of particles of the same charge. The initial densities of the electron and antiproton plasmas are given as a fraction of the total initial density. This fraction is equal to the portion of antiproton and electron particles over the total number of particles. The plasmas are loaded given their initial density distribution, with a chosen number N_l of virtual macroparticles and total effective charge Q . The two plasmas are then managed separately with respect to their different plasma parameters (i.e. mass, charge). The macroparticles loaded are confined by the potential well. For the purpose of this study, the electrode voltage can be set to a value at each iteration allowing to simulate the voltage variation of the e-kick.

Throughout the simulation, the position and velocity of the macroparticles are updated. The updated state of the plasma is found by integrating the Newton equation of motion using the leapfrog algorithm [7] (see Fig. 3):

$$m \frac{\mathbf{v}_{p,new} - \mathbf{v}_{p,old}}{\delta t} = \mathbf{F}_{old} = q\mathbf{E}, \quad (5)$$

$$\frac{\mathbf{z}_{p,new} - \mathbf{z}_{p,old}}{\delta t} = \mathbf{v}_{p,new}, \quad (6)$$

where q is the charge of the macroparticle, δt is the time increment, \mathbf{F}_{old} the force acting on the macroparticle, \mathbf{z}_p is the axial position, \mathbf{v}_p the velocity and m the weighted mass of the macroparticles. The electric field \mathbf{E} is obtained at each iteration as

$$\mathbf{E} = - \left[\frac{\partial \phi}{\partial z} \right], \quad (7)$$

hence the electric field at each grid point can be obtained using Taylor series:

$$\mathbf{E} = - \left[\frac{\phi(r, z + h_z) - \phi(r, z - h_z))}{2h_z} \right]. \quad (8)$$

The system of equations 5 and 6 is solved to find the variables noted by the subscript 'new' at time $t + \delta t$ referring to the updated state of the macroparticle calculated using the 'old' variables from the previous iteration.

The charge density used to solve the Poisson equation is obtained by projecting the macroparticle positions onto the discrete grid. This is done by considering the macroparticles as uniformly charged clouds of single-cell size in the grid (see Fig. 4). This process requires a weighting of the charges at the grid points. For a macroparticle at position z_i with charge q_c between two grid points at Z_j and Z_{j+1} , we can show that the charge assigned to j is

$$q_j = q_c \left[\frac{Z_{j+1} - z_i}{h_z} \right] \quad (9)$$

and the charge assigned to $j + 1$ is

$$q_{j+1} = q_c \left[\frac{z_i - Z_j}{h_z} \right]. \quad (10)$$

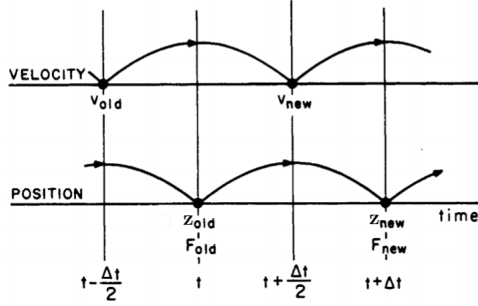


Figure 3. Sketch of the leapfrog integration method. The simulation computes the position and the velocity at interchanging times. Figure adapted from [7].

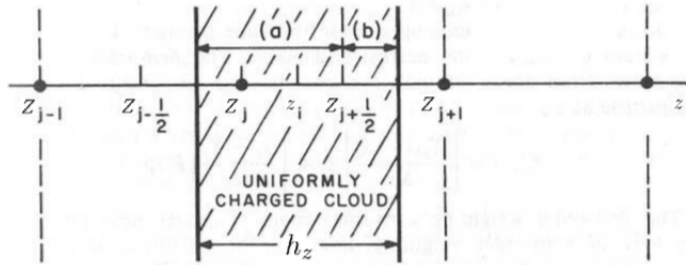


Figure 4. Effective shape of a macroparticle in the grid following the method known as first-order particle weighting. This weighting gives the part of the cloud that is in the j th cell at Z_j and the part which is in the $(j + 1)$ th cell at Z_{j+1} . Figure adapted from [7].

The total effective charge Q_j on each grid point j is computed by calculating the weight of each macroparticle. The discrete charge density $n(r, z)$ at each grid point is then $Q_j/W(r)$, where $W(r)$ is the effective 3D volume of a grid cell at radius r as shown in Fig. 5.

$$W(r) = \begin{cases} \frac{1}{4}\pi h_r^2 h_z, & \text{if } r = 0 \\ 2\pi h_r h_z, & \text{otherwise.} \end{cases}$$

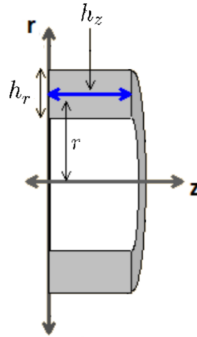


Figure 5. Effective 3D volume $W(r)$ of a grid cell. This also represents the effective shape of a macroparticle in three dimensions. At $r = 0$, it is just a cylinder with radius $h_r/2$. Taken from [6].

The time step of the simulation is chosen with respect to the plasma electron frequency ω_p of the plasma. The plasma frequency is the fastest rate at which the charge density can oscillate in a plasma. The plasma frequency is expressed as

$$\omega_p = \left(\frac{n_0 e^2}{\epsilon_0 m} \right), \quad (11)$$

where n_0 is the density of the plasma, m and e is the mass and charge of the macroparticle, respectively. To resolve the plasma frequency, the time step was chosen to be smaller than the plasma period by a factor of at least 25.

3.2 Loading Procedure

The loading procedure consists of finding the initial charge density of the plasma and placing the macroparticles according to this initial charge density on the grid.

3.2.1 The Poisson Boltzmann Equation for Plasma in Equilibrium

A procedure to obtain an equilibrium distribution that mimics the plasma inside the ALPHA trap is implemented in this project. A cold non-neutral plasma such as the electron plasma used in ALPHA is assumed to have a plasma density following the Boltzmann distribution [18; 19; 20]. The Poisson Boltzmann distribution predicts the collective behaviours of systems at thermodynamic equilibrium as a function of their constituent parts. The particles inside a plasma come to thermal equilibrium with each other through Coulomb collisions while confined by static electric and magnetic fields. The Poisson-Boltzmann equation is used to calculate the self electric potential created by charged particles inside a non-equilibrium thermal plasma described by the Boltzmann distribution. The self electric potential is used to compute the electrostatic interactions between particles. The Poisson-Boltzmann equation for a cylindrical geometry is given by

$$\frac{1}{r} \frac{\partial}{\partial r} \left(r \frac{\partial \phi}{\partial r} \right) + \frac{\partial^2 \phi}{\partial z^2} = \frac{N_0}{\epsilon_0} \exp \left(\frac{-[-e\phi(r, z) + \frac{1}{2}m\omega(\Omega - \omega)r^2]}{k_b T} \right), \quad (12)$$

where Ω is the cyclotron frequency, ϕ the electric potential, e , m and v are the particle charge, mass and velocity, respectively. The parameters N_0 , T and ω are the total number of particles, the energy and the canonical angular momentum in the system, respectively [19]. The second term in the exponential accounts for the rigid rotation of the plasma column due to the cyclotron motion and the $E \times B$ drift. In the case of a cylindrical trap and a finite plasma, the numerical solution of Equation [12] is obtained through the convergence of an iteration procedure. Here follows the details of the method used to solve this nonlinear partial differential equation. The Poisson-Boltzmann equation is solved in local equilibrium using experimental data of the radial distribution obtained at CERN. Hence, we can ignore the second exponential term in Equation [12]. The information on the radial distribution of the plasma inside the trap is obtained thanks to the combination of a micro-channel plate (MCP) camera and a phosphor screen as shown in Fig. 6. At the end of a trapping procedure, the plasma is dumped outside the trap. When a particle of the plasma hits one of the channels, it produces secondary electrons. These electrons are then accelerated towards the phosphor plate thanks to the voltage difference between the front and back of the MCP. The phosphor screen emits visible light which is then captured by a Charged Coupled Device (CCD) camera creating a false-color 2D image of the axially-integrated plasma densities [14].

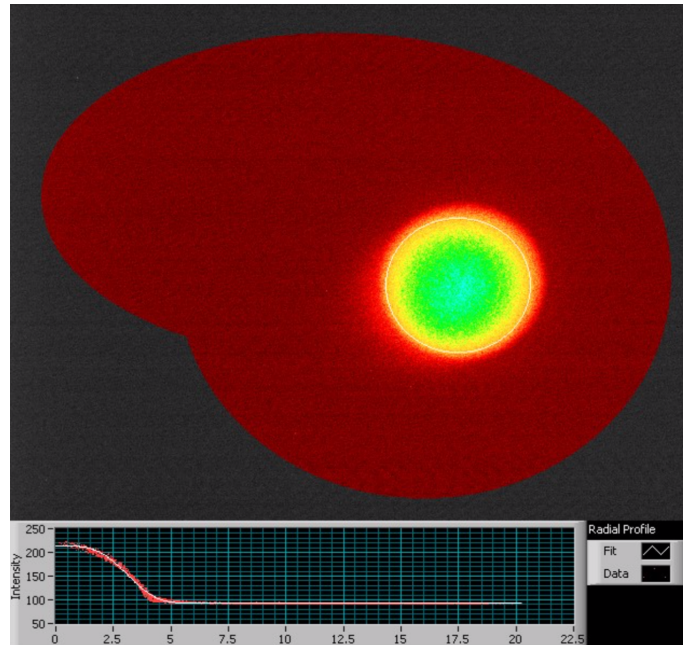


Figure 6. Example of an MCP image for an electron plasma, integrated along the axial direction. The image is obtained as the plasma exits the potential well, giving an idea of the distribution of the plasma that was previously sitting in the trap. The high and low intensities are represented in green and red, respectively. The radial profile fit which relates the brightness of the plasma to its distance from the center is shown at the bottom of the picture (x-axis in mm). For this plasma, the fit parameters read $a = 1.218 \times 10^2$, $c = 3.549$, $b = 0.3442$ and $r_0 = [21.45, 14.23]$ mm. The fit is precise at about 90 percent [14].

The data is empirically fitted to a generalised Gaussian function of order c

$$I(r) = a \exp \left[-\frac{|r - r_0|^c}{b} \right], \quad (13)$$

where a is an arbitrary constant of proportionality with the brightness at the center, b is the radius of the plasma inferred by the radial intensity distribution and r is the distance from the center r_0 . In this project, the parameters b and c are found from empirical studies. In the model, the value r_0 is set to zero as the plasma is assumed to be in the center. The value of a is chosen to satisfy the normalisation conditions as explained below. A Faraday cup detector is used to measure the charge deposited by electrons, from which their number can be inferred.

The iterative process to find the initial density is performed as follows:

1. The region of interest for the density is defined by the limits of the trapping well. All the grid points outside the trapping region are set to the same potential as the limiting grid points. In this study, the region of interest is located in the center of the trap between 0.02 m and 0.045 m along the axial direction of the trap as shown in Fig. 7.

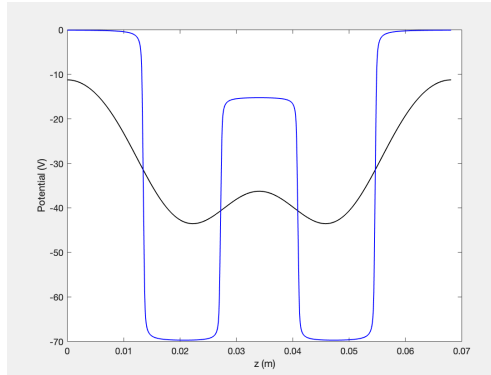


Figure 7. Potential well used prior to the e-kick (side view). The shape of the voltage is based on experimental data. The potential along the z axis at the center of the trap (black) and at the electrode wall (blue) is displayed.

2. The procedure is initialized by estimating the starting equilibrium density that satisfies the thermal equilibrium condition at temperature T . The starting normalised density is given as

$$n(r, z) = \frac{1}{\epsilon_0} \exp \left(\frac{-[-e\phi(r, z)] - \phi_c(r, z)}{k_b T} \right), \quad (14)$$

where ϕ_c is the potential at the center of the trap and $\phi(r, z)$ is given as the solution to the Laplace equation ϕ_t .

3. An equilibrium density that satisfies the thermal equilibrium condition at temperature T is estimated. The normalised guess density is given as in Equation [14] where $\phi(r, z)$ is calculated using the starting/previous guess density as defined in Equation [1].

4. The guess density is fitted to the radial profile σ determined from the intensity distribution given in Equation [13]. The fit to the radial profile allows the rigid rotation of the plasma column (due to the $E \times B$ drift) to be taken into account. The guess density is normalised as

$$\sum_z^{N_z} n(r, z) = A\sigma(r), \quad (15)$$

where A is a normalisation constant.

5. The guess density is normalized to the total charge Q given as an input. The guess density integrated over the volume should match the total charge in the trap such that

$$\sum_r^{N_r} \sum_z^{N_z} 2\pi r n(r, z) = Q. \quad (16)$$

6. The Pseudo Kolmogorov Smirnov (KS) distance between the cumulative distribution of the starting/previous density and the guess density is estimated [21]. An example of the Pseudo KS distance between two cumulative distributions is shown in Fig. 8. The distributions are assumed to be symmetric with respect to the trap center, hence the Pseudo KS distance is chosen to be twice the normal KS distance. A stopping criterion was chosen on the Pseudo KS distance of 1×10^{-6} [21].

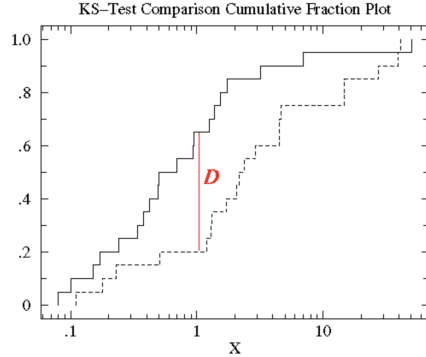


Figure 8. Schematic of the two-sample Kolmogorov–Smirnov statistics. The dashed and black lines correspond to two cumulative distribution functions. The vertical red line is the Pseudo Kolmogorov Smirnov (KS) distance. Figure taken from [22]

7. The final density solution, that will be fed into the iteration loop, is given by the linear combination of the starting/previous density and the guess density. The linear combination coefficients are equal to the Pseudo KS distance between the cumulative distribution of the starting density and the first guess density d_{ks} , and the distance $1 - d_{ks}$. The values of the coefficients indicate how low or high the temperature is (i.e. how much of the new guess would be necessary to add to the previous guess).

At the end of the iterative procedure, the macroparticle number density $n(r, z)$ and the potential $\phi(r, z)$ is calculated and extracted as outputs [23].

3.2.2 Loading the Particles on the Grid

Several methods to load the particle in a PIC code exist. One of the approaches is explored in the MATLAB code written by Federico Peinnetti [3; 24]. His method assigns an initial phase-space position to each macroparticle (z_p, v_p) and a charge weight to each macroparticle (q_p). This is done by respectively inverting the velocity density distribution and the cumulative charge of the plasma. This method reduces the propagation of non-physical density fluctuations and instabilities inside the plasma. The equilibrium distribution aims at representing the experimental conditions in the laboratory [3; 7; 18].

An alternative version of the loading is used in this study and presented below. The method assigns an initial space position to each macroparticle (z_p) to match the charge density found by solving the Poisson-Boltzmann equilibrium. The number of macroparticles N_l and the total charge Q desired is configured at the beginning of the simulation. The initial charge density $n(r, z)$ in thermodynamic equilibrium is saved to file for a number of macroparticles and a given charge. The initial densities of the electron and antiproton plasmas are given as a fraction of the total initial density. This fraction is equal to the portion of antiproton and electron particles over the total number of particles. The grid point density at each radius r is multiplied by the volume $W(r)$ to give the necessary total charge of each radius $\mu(r)$.

This code requires that each macroparticle has to have the same contribution to the charge density $n(r, z)$ at any radius. For instance, the charge of a particle at a higher radius must be larger than the ones at a lower radius as its volume is larger. It was decided to ensure that there are enough particles at each radius to describe the plasma behaviour.

The relation between v_0 , the effective volume at radius equal 0 and v_r the effective volume at radius r (see section 3.1) is such that

$$\frac{v_0}{v_r} = \frac{1}{8 * r}. \quad (17)$$

Hence, the macroparticle charge at each radius was weighted accordingly such that

$$q_c(r) = \begin{cases} q, & \text{for } r = 0 \\ q * r * 8, & \text{for } r \neq 0 \end{cases}$$

where q is the charge at radius equal zero. The charge q is found by dividing the total charge in the trap by the total number of macroparticles. The total charge is computed by weighting the total charge at each radius with respect to the volume.

Hence, the number of macroparticles required at each radius is calculated to be

$$\mu(r) = \frac{Q_r(r)}{q_c(r)}, \quad (18)$$

where r is the index of the radius.

In order to be appropriately normalised, the following equality must hold

$$\sum_r^{N_r} \mu(r) = N_t. \quad (19)$$

The macroparticles are placed on the grid at each radius by inverting the cumulative density distribution [7]. The particles are distributed uniformly along the radius.

A Boltzmann distribution function is chosen for the distribution of the macroparticles' velocity to satisfy thermal equilibrium condition. The distribution of velocities is given as followed:

$$f(v) = \left(\frac{m}{2\pi k_b T}\right)^{\frac{3}{2}} e^{\left(-\frac{mv^2}{2k_b T}\right)}, \quad (20)$$

where m is the mass of the macroparticles, T the temperature of the plasma, and v the velocity of the macroparticles.

3.3 Diagnostics

To perform diagnostics, the velocities and positions of the macroparticles are saved during the simulation at specified times. A variety of saving methods are available. The states can be saved at any chosen time step of the simulation depending on the study of interest. Moreover, the state of the macroparticles at a specified radius r can be saved. The trap and plasma parameters are exported to a '.csv' file. The trap potential and the self potential data are also available as a '.csv' file.

3.3.1 Energy Calculations

PIC simulations presently conserve either momentum or energy [25]. The leapfrog method described in the previous section 3.1 functions as a symplectic integrator. This algorithm allows the energy conservation of the model [7].

The total energy of plasma is given by the kinetic energy T and the potential energy U of the plasma [26].

$$E = T + U. \quad (21)$$

The kinetic energy of the particles can be found as

$$T = \sum_{k=i}^{N_p} \frac{1}{2} m_i v_i^2, \quad (22)$$

where N_p is the number of macroparticles, m_i is the mass and v_i the velocity of the macroparticles.

When the plasma is confined, both the potential energy of the well and the self-consistent energy contribute to the total potential energy U such that

$$U = U_s + U_t, \quad (23)$$

where U_s is the self-potential energy and U_t is the total potential energy from the well.

Inside the PIC code, the solution to the well and self potential are discrete at each grid point. For a macroparticle at position z between two grid points Z_j and Z_{j+1} at radius R with charge $q_c(r)$, the potential $\phi_t(z, r)$ acting on the macroparticle is calculated as a linear interpolation of the potential at the grid points Z_j and Z_{j+1} . Hence, the total potential energy from the well is given by

$$U_t = \sum_{k=1}^{N_p} q_c(r_k) \phi_t(z_k, r_k), \quad (24)$$

where N_p is the total number of macroparticles, r_k the radius and z_k the position along the z-axis of macroparticle k . The total self potential energy inside the trap can be found as

$$\begin{aligned} U_s &= \sum_{k=1}^{N_p} q_c(r_k) \Phi_{\text{correct}}(z_k, r_k) \\ &= \sum_{k=1}^{N_p} q_c(r_k) (\varphi_s(z_k, r_k) - \varphi_{\text{single}}(z_k, r_k)), \end{aligned} \quad (25)$$

where N_p is the total number of macroparticles, q_c is the charge, z_k the position along the axial axis and r_k the position along the radius of the macroparticle k [25]. The self potential φ_s at all the grid points is obtained by solving the Poisson equation for all the macroparticles. For a macroparticle at position z between two grid points at Z_j and Z_{j+1} at radius r with charge $q_c(r)$, the potential $\varphi_s(z, r)$ acting on the macroparticle is calculated as a linear interpolation of the self potential at Z_j and Z_{j+1} . However, the self potential φ_s , at Z_j and Z_{j+1} accounts for the effect of the macroparticle on itself. Hence, a potential correction for the single particle needs to be applied. Using a symmetry argument, the potential correction of a single particle φ_{single} at a fixed radius r and axial position z can be derived to be

$$\varphi_{\text{single}}(z, r) = (w_1^2 + w_2^2) \varphi_{1,1,\text{single}}(z, r) + w_1 w_2 \varphi_{2,1,\text{single}}(z, r), \quad (26)$$

with

$$w_1 = \frac{d_1}{h_z} \quad (27)$$

and

$$w_2 = (1 - w_1). \quad (28)$$

As shown in Fig. 9, $\varphi_{1,1,\text{single}}$ refers to the potential that a particle experiences at grid point 1, from a particle placed at grid point 1. $\varphi_{2,1,\text{single}}$ refers to the potential that a particle experiences at grid point 2, from a particle placed at grid point 1. We assume that the solution to $\varphi_{1,1,\text{single}}$ and $\varphi_{2,1,\text{single}}$ is equivalent throughout the region of interest (defined in section 3.2.1) along the z axis. We also assume that the particle is positioned at a radius corresponding exactly to the grid point r . The form of $\varphi_{1,1,\text{single}}$ and $\varphi_{2,1,\text{single}}$ needs to be evaluated at all radii.

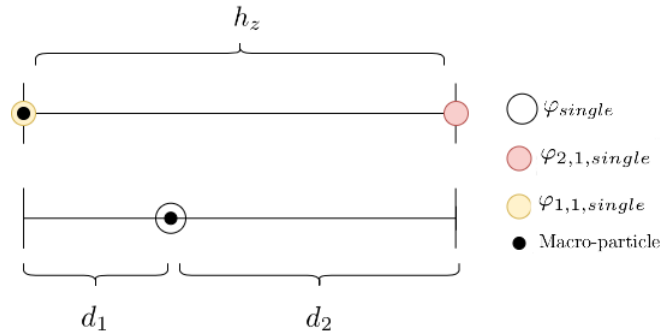


Figure 9. Schematic representation of the interpolation of the potential experienced by a macroparticle between two grid points

As shown in Fig. 10, it is found that the correction energy to the self potential energy (orange) is negligible compared to the total self energy (purple). Hence, it can be ignored without loss of accuracy.

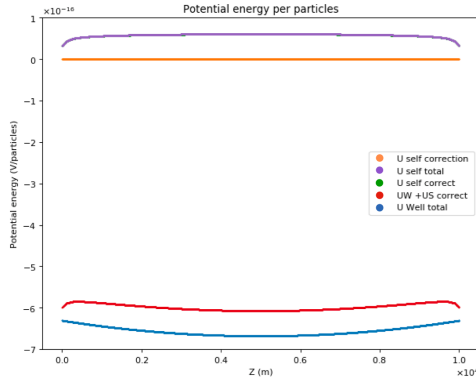


Figure 10. Schematic of the potential energies per grid point along the axial axis. The potential energy from the trap (U Well total in blue), the total self energy (U self total in purple), the correction to the self potential energy (U self correction in orange), the corrected potential energy (U self correct in green - not visible as overlaid by the purple one) and the total potential energy corrected (UW+US correct in red) are shown on the plot.

3.3.2 Plasma Dynamics Diagnostics

The following diagnostics were developed to get an insight into the plasma dynamics. An example of the diagnostics implemented is given at a fixed time t in Fig. 11a and Fig. 11b for antiprotons and electrons, respectively. A detailed description of the diagnostics implemented is given below:

- The positions and velocities of the macroparticles are displayed on a phase space diagram at time t and radius r in the bottom left corner of Fig. 11a and 11b. Each red dot represents a macroparticle of the plasma.
- The density distribution at radius r at time t is also displayed. The density is obtained for each grid point as explained in section 3.1. The red line on the top left corner plot of Fig. 11a and 11b is the value of the initial density obtained by solving the Poisson Boltzmann equation at each grid point. It ensures that the macroparticles were loaded appropriately and accurately as described in section 3.2.1.
- Information on the simulation parameters such as the saved state time t , the radius r , and the number of macroparticles can be found on the top right corner of the simulation.
- On the bottom right corner, the velocity distribution of macroparticles at time t and radius r is shown as a histogram.

The saved states data are displayed successively as saved during the simulation to create a video (gif) of the evolution of the plasma. This gives insights on the dynamical evolution of the plasma over time. These diagnostics are crucial in determining whether the plasma is in thermal equilibrium.



Figure 11. Visualisation of the plasma parameters and properties at time $t = 4.48 \times 10^{-8}$ s of the plasma evolution with iteration time step $\delta t = 0.1$ ns and at radius $r = 0$. There are 9 million electrons and 100 000 antiprotons in the trap. The simulation is using 8075 macroparticles. The Debye length for the electron plasma (a) is approximately 9×10^{-5} m, and the plasma frequency approximately 220 MHz. For the antiprotons (b) the Debye length is approximately 4×10^{-4} m and the plasma frequency approximately 1.5 MHz. The grid spacing is small enough to resolve the electron plasma Debye length ($N_z=775$ and $N_r=170$).

3.3.3 Temperature

Any temperature measurement in this report is calculated as presented below. The temperature diagnostic uses the equipartition theorem given as [27]

$$\sum_i^{N_l} \frac{1}{2} m_i(r) \bar{v}_i^2 = N_l k_b T, \quad (29)$$

where T is the temperature of the plasma, k_b the Boltzmann constant, and N_l is the total number of macroparticles in the plasma. The mass $m_i(r)$ of the macroparticle i at radius r is weighted as discussed in section 3.2.1. The average velocity $\bar{v}_i(t)$ at time t of the macroparticle i is calculated from the average of the particle velocities at time t and $t + 1$. By rearranging the Equation [29] for T , the average kinetic energy in Kelvin at time t is obtained. These energies at each time t are then averaged over the total time of the saved states. Note that this is not a direct measurement of the temperature of the plasma.

This measurement gives an insight into the temperature of the plasma. One has to take into account the statistical limit of this diagnostic for radiiuses with a small number of macroparticles. The term ‘average kinetic energy’ will be employed to qualify all the measurements made with this diagnostic.

On Fig. 11a and 11b, the average temperature of the plasma and the radius are displayed on the top right corner. The distribution of particle velocities is fitted with a Boltzmann distribution (Equation [12]) with the calculated temperature T . The red line on the bottom right corner plot of Fig. 11a and 11b is the Boltzmann distribution of velocities obtained with temperature T .

3.4 Simulating the e-kick

The simulated geometry was chosen to match the experimental trap. The trap is modeled with identical electrodes of length 13.22 mm and diameter 29.76 mm separated by a gap of 0.5 mm. The electrodes’ potential was chosen in agreement with empirical studies [14]. The resulting potential well shape is shown in Fig. 7. The voltage of the central electrode (i.e. electrode 3) is modified as a step function for the center e-kick. The voltage of one of the side electrodes is modified as a step function for the side e-kick. The side electrodes correspond to the electrodes at the edge of the trapping well (i.e. electrode 2 or 4) as shown in Fig. 7.

To smooth the edge of the step function and avoid non-physical heating, a sigmoid curve is used. The shape of the sigmoid curve is given as

$$sig(t) = (V_f - V_0) \frac{1}{1 + \exp\left(\frac{-2g(t-\frac{d}{2})}{d}\right)} + V_0, \quad (30)$$

where V_0 is the initial voltage, V_f is the final voltage, t is time in second, d is the duration over which the voltage is raised or lowered, g determines the accuracy of the rise. For instance, for a value of $g = 4.5$, the voltage rises to 98 % of the final voltage V_f after duration d .

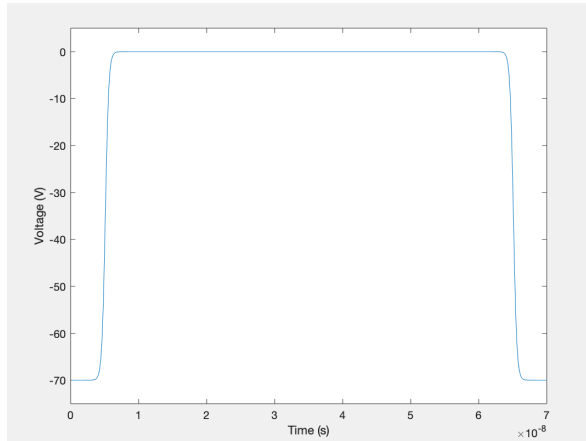


Figure 12. Example of the sigmoid variation of the trap central electrode’s potential over time used during the central e-kick. The duration, d , over which the voltage is raised or lowered is equal to 10 ns. The voltage is changed from -70 V to 0 V. After a delay time $\tau = 50$ ns the potential is lowered back to -70 V

The sigmoidal potential variation of the central electrode is shown in Fig. 12. The parameters V_f , d , and the delay time τ will be varied during the study of the e-kick.

4 RESULTS AND DISCUSSION

Multiple versions of the simulation of the e-kick were performed for an electron/antiproton plasma in equilibrium inside a Penning-Malmberg trap. A comparative study between the central electrode e-kick and the side electrode e-kick was performed.

4.1 Test of the Thermal Equilibrium of the Plasmas

The thermal equilibrium parameters of the plasmas were chosen in accordance with the experimental data. For each plasma, the thermal equilibrium was tested and the results are reported in this section. Note that the physical properties of the plasma, the Debye length, and the plasma frequency were calculated for each plasma. These properties play an important role in choosing the numerical parameters of the simulation such as N_r , N_z , and the time step as described in section 3.1 [7; 28; 29].

The values of the thermal equilibrium initial density parameters described above are given in table 1 for plasmas A, B, and C. The number of electrons, antiprotons, and macroparticles, as well as the values of parameters b and c (see section 3.2.1) are reported in the table.

Table 1. Values of the three thermal equilibrium parameters which were used for the e-kick.

	PlasmaA	PlasmaB	PlasmaC
Temperature (K)	1000	400	150
Number of electrons	9 million	2 million	150000
Number of antiprotons	100000	100000	100000
Number of macroparticles	8075	7175	3010
N_z	775	810	585
N_r	170	180	128
b	0.6	0.6	0.6
c	3.442	3.442	3.442
λ_d antiprotons (m)	9×10^{-4}	4×10^{-4}	1×10^{-4}
ω antiprotons (MHz)	0.5	0.75	3.63
λ_d electrons (m)	9×10^{-5}	9×10^{-5}	1.2×10^{-4}
ω electrons (MHz)	220	147	63

The state of plasma A at time $t = 4.48 \times 10^{-8}$ s is shown in Fig. 13a and 13b for the electrons and antiprotons, respectively. Similarly, the state of plasma B at time $t = 3.4 \times 10^{-8}$ s is shown in Fig. 14a and Fig. 14b for the electrons and antiprotons, respectively. The state of plasma C at time $t = 6.16 \times 10^{-8}$ s is shown in Fig. 15a and Fig. 15b for the electrons and antiprotons, respectively.



Figure 13. Visualisation of the plasma A parameters and properties at $N_r = 0$ and time $t = 4.48 \times 10^{-8}$ s which corresponds to 10 times the electron plasma period. The initial temperature is 1000 K. There are 9 million electrons and 100 000 antiprotons in the trap. The simulation is using 8075 macroparticles. The Debye length for the electron plasma (a) is approximately 9×10^{-5} m and the plasma frequency 220 MHz. For the antiprotons (b), the Debye length is approximately 9×10^{-4} m, and the plasma frequency 0.5 MHz. The grid spacing is small enough to resolve the electron plasma Debye lengths ($N_z = 775$ and $N_r = 170$).



Figure 14. Visualisation of the plasma B parameters and properties at $N_r = 0$ and time $t = 3.4 \times 10^{-8}$ s which corresponds to 5 electron plasma period. The initial temperature is 400 K. There are 2 million electrons and 100 000 antiprotons in the trap. The simulation is using 7175 macroparticles. The Debye length for the electron plasma (a) is approximately 9×10^{-5} m and the plasma frequency 147 MHz. For the antiprotons (b), the Debye length is approximately 4×10^{-4} m and the plasma frequency is 750 kHz. The grid spacing is small enough to resolve the electron plasma Debye lengths ($N_z = 810$ and $N_r = 180$).



Figure 15. Visualisation of the plasma C parameters and properties at $N_r = 0$ and time $t = 6.16 \times 10^{-8}$ s in the simulation. The initial temperature is 150 K. There are 150000 electrons in the trap. The simulation is using 3010 macroparticles. The Debye length of the electrons was calculated to be approximately 1.2×10^{-4} m and the plasma frequency approximately 63 MHz. For the antiprotons (b), the Debye length is approximately 1×10^{-4} m and the plasma frequency is approximately 3.63 MHz. The grid spacing is small enough to resolve the Debye lengths ($N_z = 585$ and $N_r = 128$).

Throughout the simulation, we observe that macroparticles remain in the same region where they are loaded, indicating that the plasma in thermal equilibrium is well confined by the trapping potential. The average temperature displayed on the graphs indicates that the average kinetic energy of all the plasmas varies by less than 10 percent of their initial density temperature.

4.2 Center Electrode E-kick

The central e-kick is performed by lowering the potential of the central electrode as described in Equation [30] with a lowering time of 10 ns. The potential of the central voltage was modulated from an initial voltage $V_i = -15$ V to a final voltage V_f that varies for the different plasmas. The voltage was modified by steps of ΔV . A voltage of V_f high was chosen for each plasma as a threshold voltage where no electrons leave the trap. Note that when the threshold voltage V_f high equals the initial trapping voltage, the plasma is not very well confined by the trapping voltage. Moreover, the voltage V_f low threshold is defined such that no antiprotons leak outside of the trap (a lower voltage could lead to the leaking of antiprotons).

The values of the central e-kick parameters described above are given in table 2 for plasmas A, B, and C. The plot of the potential well with the central electrode voltage lowered to $V = -40$ V is shown in Fig. 16. The central electrode potential is kept low for a delay time τ allowing the electrons to escape the trapping region. The delay time τ was varied between 0 and 90 ns by steps of 10 ns. The time step of 1×10^{-10} s and the delay time was chosen to resolve the plasma frequency of the 3 initial densities. Finally, the central electrode potential is raised back to the initial trapping voltage V_i according to the sigmoid Equation [30].

Table 2. The values of the thermal equilibrium parameters of plasmas A, B and C used for the central e-kick.

	PlasmaA	PlasmaB	PlasmaC
V_f low (V)	-70	-79	-79
V_f high (V)	-15	-30	-30
ΔV (V)	1	1	1

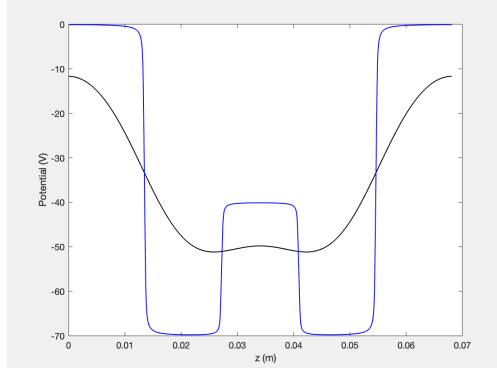


Figure 16. Potential well used for the central e-kick with the central electrode set to $V = -40$ V. The potential along the z axis at the center of the trap (black) and at the electrode wall (blue) is displayed.

The results of the central e-kick are shown as contour plots in Fig. 17, Fig. 18 and Fig. 19 for plasma A, B and C, respectively.

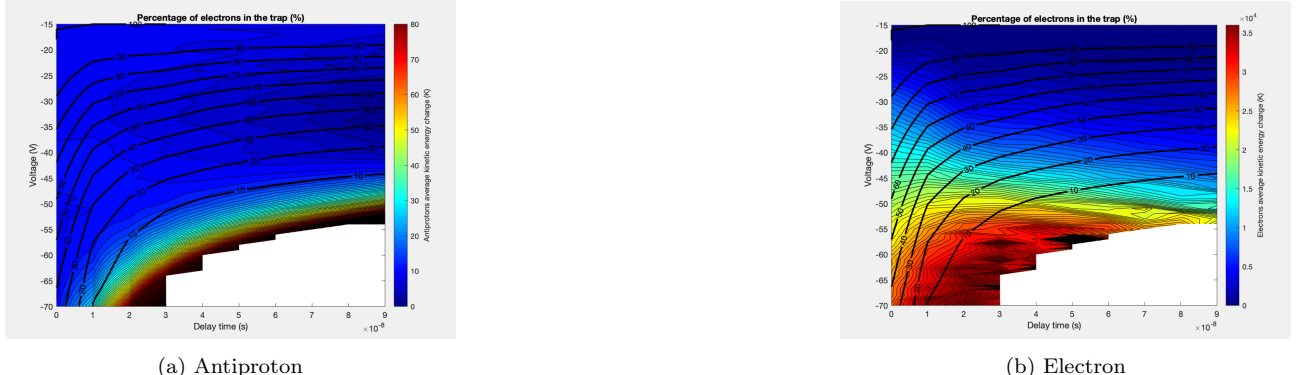


Figure 17. Contour plot of the percentage of electrons of plasma A in the trap after the central e-kick as a function of the final voltage and the delay time. The differences in average kinetic energy compared to the initial loading temperature of the antiproton (a) and electron (b) plasmas are displayed as a color gradient.

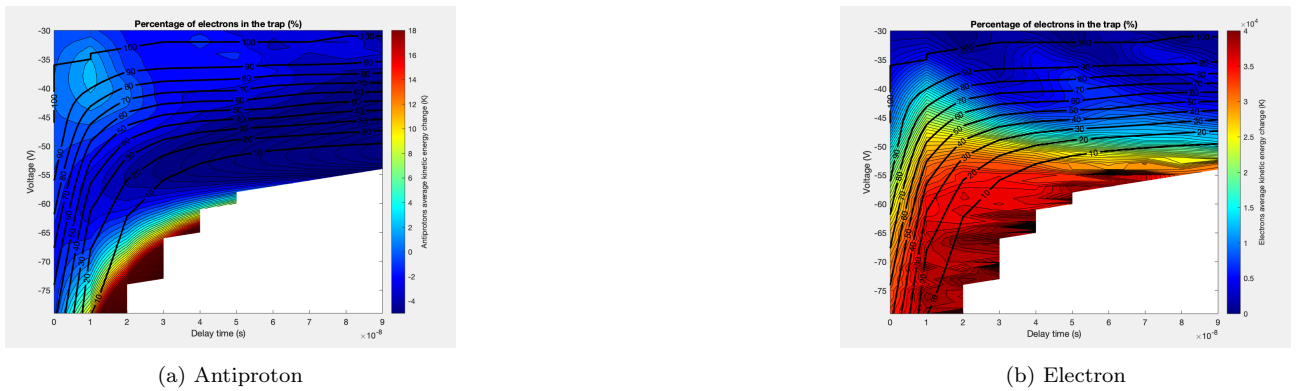


Figure 18. Contour plot of the percentage of electrons of plasma B in the trap after the central e-kick as a function of the final voltage and the delay time. The differences in average kinetic energy compared to the initial loading temperature of the antiproton (a) and electron (b) plasmas are displayed as a color gradient.



Figure 19. Contour plot of the percentage of electrons of plasma C in the trap after the central e-kick as a function of the final voltage and the delay time. The differences in average kinetic energy compared to the initial loading temperature of the antiproton (a) and electron (b) plasmas are displayed as a color gradient.

The percentage of electrons left compared to the initial number of electrons, 100 ns after the e-kick, is represented as black contour lines. The temperatures of the antiproton and electron plasmas inside the trap are computed as the average kinetic energy of the particle over 100 ns after the e-kick. The differences in average kinetic energy compared to the initial loading temperature are represented as colored contour lines. A gradient of colors is used to emphasize the changes in average kinetic energy. The limits of the color gradient are chosen to highlight the average kinetic energy changes where electrons leave the trap. When more than 95 percent of the electrons have left the trap, the average kinetic energies are set to zero and appear in white on the contour plots.

4.3 Side Electrode E-kick

In a similar fashion as the center e-kick, the side e-kick is performed by raising the potential of the side electrodes of the trapping well (i.e. electrode 2 or 4). The potential is raised in 10 ns. The potential of the side voltage was modulated from an initial value $V_i = -70$ V to a final voltage V_f that varies for the different plasma. The voltage was modified by steps of ΔV . Inversely to the center e-kick, the voltage of V_f low was chosen for each plasma as a threshold voltage where no electrons leave the trap. Moreover, the voltage V_f high threshold is defined such that no antiprotons leak outside of the trap (a higher voltage could lead to the leaking of antiprotons). The voltage is changed by steps of $\Delta\tau$.

A picture of the potential well with the side electrode voltage raised to $V = -20$ V is shown in Fig. 20.

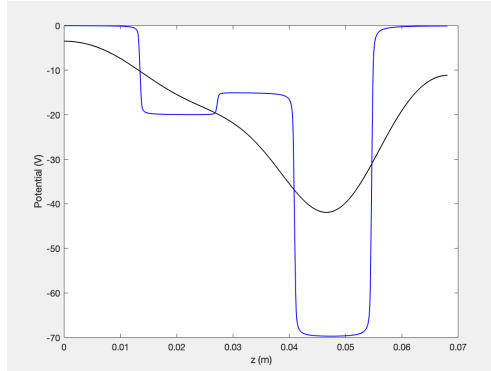


Figure 20. Potential well used for the side e-kick with the side electrode set to $V = -20$ V. The potential along the z axis at the center of the trap (black) and at the electrode wall (blue) is displayed.

The side electrode potential is kept high for a delay time τ allowing the electron to escape the trapping region. The delay time τ was varied between 0 and τ_f ns by steps of $\Delta\tau$. The time step and the delay time were chosen such that the plasma frequency is equal to 25 times the time step. The delay time was chosen to resolve the plasma frequency of the 3 initial densities. Finally, the side electrode potential is raised back to the initial trapping voltage V_i as described in Equation [30]. The values of the side e-kick parameters described above are given in table 3 for plasmas A, B, and C. The results of the side e-kick are shown as contour plots in Fig. 21, Fig. 22 and Fig. 23 for plasma A, B and C, respectively.

Table 3. Values of the three thermal equilibrium parameters which were used for the e-kick.

	PlasmaA	PlasmaB	PlasmaC
V_f low (V)	-70	-60	-51
V_f high (V)	24.4832	-5	-24.55
ΔV (V)	1.2768	1	0.575
τ_f (ns)	40.9	27.744	29
$\Delta\tau$ (ns)	1.08	1.632	0.616



Figure 21. Contour plot of the percentage of electrons of plasma A in the trap after the side e-kick as a function of the final voltage and the delay time. The differences in average kinetic energy compared to the initial loading temperature of the antiproton (a) and electron (b) plasmas are displayed as a color gradient.



Figure 22. Contour plot of the percentage of electrons of plasma B in the trap after the side e-kick as a function of the final voltage and the delay time. The differences in average kinetic energy compared to the initial loading temperature of the antiproton (a) and electron (b) plasmas are displayed as a color gradient.



Figure 23. Contour plot of the percentage of electrons of plasma C in the trap after the side e-kick as a function of the final voltage and the delay time. The differences in average kinetic energy compared to the initial loading temperature of the antiproton (a) and electron (b) plasmas are displayed as a color gradient.

The percentages of electrons left compared to the initial number of electrons are recorded one electron plasma period after the e-kick and represented as black contour lines. The temperatures of the antiproton and electron plasmas inside the trap are computed as the average of the kinetic energy of the particle over one electron plasma period after the e-kick. The differences in average kinetic energy compared to the initial loading temperature are represented as colored contour lines. A gradient of colors is used to emphasize the changes in average kinetic energy. The limits of the color gradient were chosen to highlight the average kinetic energy changes where electrons leave the trap. When more than 95 percent of the electrons have left the trap, the average kinetic energies are set to zero and appear in white on the contour plots.

4.4 Comparative Study

For both central and side e-kick more electrons leave the trap for larger voltage drops at a given delay time. The same trend can be observed with the increase of the delay time for a given voltage. For the center e-kick, the rate at which the electrons leave the trap depends on the frequency of the plasma since the time step and delay time are the same for all the different plasmas. Hence, contour lines close to each other indicate electrons leaving at a faster rate.

In both experiments, the average kinetic energy of the plasmas increases for a decreasing number of electrons in the trap. The antiprotons heat up significantly more for the side e-kick. For the center e-kick, the antiproton plasma average kinetic energy in Kelvin increases by less than 10 percent of their initial loading temperature. For the side e-kick, the antiproton plasma average kinetic energy in Kelvin increases from a few percent up to the triple of their initial loading temperature.

For the side electrode e-kick, the antiproton average kinetic energy increases regardless of the voltage for larger delay time. Also, all the side electrode e-kick contour plots suggest that the lowest average kinetic energy for the antiprotons, regardless of the percentage of electrons in the trap, is obtained with a smaller change with respect to the initial voltage. In other words, a fast and strong kick is better than a smooth and long kick.

For the central electrode kick, a longer delay time allows more electrons to leave the trap which leads to the heating of the antiproton plasma. Moreover, for all the initial densities at any delay time, large kicks seem to increase the average kinetic energy of the antiprotons. There are no characteristic average kinetic energy trends for the initial densities that hold regardless of the number of electrons in the trap. For plasma A, a long delay time and a small voltage drop minimize the antiproton average kinetic energy for any number of electrons in the trap. For plasma B, a long delay time and an intermediate voltage drop of -55 V seems to be optimal. Finally, for plasma C, there seems to be an intermediate interval between 10 and 40 ns and voltage between -50 V and -60 V where the e-kick is the most efficient.

The antiproton average kinetic energy singular trend in Fig. 18a is worth discussing. For plasma B, with a delay time between 10-20 ns, the average kinetic energy increases around the voltage drop between -35 V and -40 V. We investigated the basic assumption that the particle escaping the potential well might enter in resonance with the trap. This resonance effect tends to increase plasmas' temperatures. An estimate of the bounce frequency was calculated by dividing the velocity of the particle with the length of the plasma. It was found that the bounce frequency of these particles is of the order of 25 ns which is potentially creating a resonance effect as it is similar to the e-kick's period. Further research should be led to understand the exact nature of this effect.

In Fig. 18a and Fig. 19a, the negative average kinetic energy change indicates that the plasma is getting colder for some of the e-kicks. It could be the case that the plasma - once loaded - finds its thermal equilibrium at a lower temperature than the set initial density temperature. Further studies of the plasma average kinetic energy over time after the loading should be done.

For the central electrode e-kick, the fluctuations of the antiprotons average kinetic energy are small compared to the initial temperature. Therefore, it is crucial to consider that their contours could be shaped by errors. Sources of errors could come from the details of the macroparticles' behavior in the simulation or from the rearrangement of the space charge. Hence, further computation is advised to obtain information on the average kinetic energy over time. The fluctuation of the temperature over time was not investigated due to the time limits of the project.

Both e-kicks significantly heat the electrons for the three initial densities. The difference in the average kinetic energy of the electrons after the central e-kick ranges from 1×10^3 K to 1×10^5 K for all the plasmas. The average kinetic energy of the electrons is larger for the side e-kick compared to the central e-kick. The temperature measurement of the electrons when large fractions of them are removed is statistically irrelevant as explained in section 3.3.3. Hence, their temperature is set to zero once there is 5 percent of electrons left in the trap. Moreover, the chaotic trend of the electron average kinetic energy, when there is a low number of them in the trap, should be ignored.

An electron's average kinetic energy trend is observed for both kicks with different initial distributions. For larger delay times, the electron average kinetic energy is minimized, regardless of the percentage of electrons in

the trap. Moreover, the lowest average kinetic energy, regardless of delay time is obtained with a smaller change with respect to the initial voltage. In other words, a smooth and long kick is better than a fast and strong kick. The electron temperature is of interest in experimental research where multiple e-kicks are done allowing the temperature of the electron/antiproton plasmas to re-equilibrate to thermal equilibrium between e-kicks. A lower temperature leads to a shorter amount of waiting time and fewer instabilities. Note that multiple e-kicks are not allowed in this simulation as the plasma is collisionless and the particles are not able to radiate energy through cyclotron radiations. The final temperature of the electrons gives an indication of what the temperature would be after thermalization.

The heating of the antiprotons and electrons comes from details of the voltage manipulation and the change in self-potential from the removal of the electrons. For instance, in the side electrode experiment, the large average kinetic energy can be explained by a push from the re-establishing trapping well as some of the electrons were leaving the trap. It is important to point out that the trap is longer than the confining region. Hence, when the velocities are saved, some macroparticles have escaped the confining well but not the trap. Technically, these macroparticles should not be accounted for in the calculation of the average kinetic energy. This effect increases the average kinetic energy of the plasma and needs to be accounted for as an error on the presented results.

Overall, the central e-kick seems to be more efficient than the side e-kick as the final energy in the trap is minimized. The center e-kick is advisable for the last e-kick procedure that removes all the electrons, and where no thermal equilibration with the electrons is possible. For the e-kick procedures that leave some of the electrons in the trap, the contour lines of both experiments can be used to find the most efficient e-kick that minimizes the electron and antiproton average kinetic energy. The optimized e-kick would be located where the contour lines intersect for a minimum number of electrons in the trap while minimizing the electron and antiproton average kinetic energy.

5 CONCLUSIONS

A PIC model has been developed in C++ to simulate the processes performed at CERN in the ALPHA experiment in which antiprotons are separated from a cold electron plasma. The preliminary steps of the development of the C++ code are summarized in this report and can be found in detail in Daniel Duque's report [6]. An explanation of the iterative method used to determine the initial density distribution of the plasma is given. An algorithm that appropriately loads the macroparticles to match the initial conditions was implemented. All component parts of the program have been tested separately and as a whole to produce results that are in good agreement with both theoretical and experimental results. Various methods and diagnostics relevant to the study of the e-kick were developed (i.e. energy diagnostics and temperature diagnostic). This model was successfully used to perform a detailed study of the electron removal process using both the central and side electrodes.

The average kinetic energy of the plasma is measured in Kelvin to estimate the temperature of the plasma. It was found that the e-kick leads to the heating of both the electron and antiproton plasmas. The antiprotons average energy after the e-kick is larger for the side e-kick. For the center e-kick, the average kinetic energy increases by less than 10 percent of the initial temperature whereas for the side e-kick the average kinetic energy increases up to the triple of the initial temperature. For the side e-kick, a fast and strong kick minimises the average kinetic energy of the antiprotons. The electron plasma is heated to a high average kinetic energy ranging between 1×10^3 K and 1×10^5 K for both e-kicks regardless of the initial distribution temperature. A smooth and long kick minimises the average kinetic energy of the electrons for both e-kick types. The temperature of the electrons after the e-kick is of interest in experimental research where multiple e-kicks are done. It gives an insight into the temperature of the antiproton/electron plasma after thermal re-equilibration post e-kick. Overall, the central e-kick seems to be more efficient than the side e-kick as the final energy in the trap is minimised. These results could be used to guide experimental study in the ALPHA experiment taking into account the assumptions and simplifications made in the model.

Further investigation of the plasma temperatures after an e-kick with varying well depths, plasma types and voltage rise times could be led. The fluctuation of the temperature over time should be investigated as well. These would give further understanding of the plasma behaviour during the e-kick procedure. Additionally, taking advantage of the dimensionality of the grid, the distribution of the temperature along the radial direction could be studied. Finally, an initial loading of further complexity can be envisioned. For instance, a loading representing the centrifugal separation of the antiproton inside the trap can be implemented for future research [30], as this would be closer to the experimental initial loading.

ACKNOWLEDGEMENTS

I would like to express my special thanks to my supervisor Dr. William Bertsche who gave me the opportunity to do this project on the 2D PIC code for anti-matter plasmas, and who also helped me in the research.

REFERENCES

- [1] D. Möhl, "History and early achievements," *CERN-PS-99-034-DI (CERN) LEAR*, 1999. <https://cdsweb.cern.ch/record/388662>.
- [2] G. Mason and R. Spencer, "Simulations of the instability of the m=1 self-shielding diocotron mode in finite-length non-neutral plasmas," *Physics of Plasmas*, Vol.9, 2002.
- [3] Peinetti, F. and Peano, F. and Coppa,G. and Wurtele,J., "Particle-in-cell method for parallel dynamics in magnetized electron plasmas: Study of high-amplitude bgk modes," *Journal of computational physics*, Vol.218, pp. 102–122, 2006.
- [4] F. Peinetti, W. Bertsche, J. Fajans, J. Wurtele, and L. Friedland, "Numerical studies of driven, chirped Bernstein, Greene, and Kruskal modes," *Physics of Plasmas*, Vol.12, 062112, 2005.
- [5] P. Frey, "The finite difference method," *Université Sorbone Paris, Lecture notes*, pp. 79–92, 2017. https://www.ljll.math.upmc.fr/frey/cours/UdC/ma691/ma691_ch6.pdf.
- [6] D. Duque, "Plasma PIC code for use in Antihydrogen Physics," *Master Thesis at the University of Manchester, School of Physics and Astronomy*, 2020. C++ code can be found at: <https://github.com/Daniel32Duque/PIC-Trapped-Plasma>.
- [7] C. Birdsall and A. Langdon, *Plasma Physics via Computer Simulation*. CRC Press, 1st ed., 1975.
- [8] S. Maury, "The Antiproton Decelerator: AD," *Hyperfine Interactions*, Vo1.109, pp. 43–52, 1997.
- [9] T. Eriksson, "AD: low-energy antiproton production at CERN," *Hyperfine Interact*, Vol.194, p. 123, 2009.
- [10] G. Baur *et al.*, "Production of Antihydrogen," *Physics Letters*, Vol.368, pp. 251–258, 1996.
- [11] G. Amsler *et al.*, "production and detection of cold antihydrogen atoms,"
- [12] E. Butler, "Antihydrogen formation dynamics and trapping," *Ph.D. Thesis from the Department of Physics at Swansea University*, 2011.
- [13] G. Andersen *et al.*, "Evaporative Cooling of Antiprotons To Cryogenic Temperatures," *Physics Letters*, Vol.105, 013003, pp. 1–5, 2010.
- [14] B. Bottura, "E-kick potential well modifications in the ALPHA experiment at CERN," *Internship report, University of Manchester*, 2017.
- [15] C. Amole *et al.*, "The ALPHA antihydrogen trapping apparatus," *Nuclear Instruments and Methods in Physics Research*, Vol.735, pp. 319–340, 2013.
- [16] J. Bordón, J. Aznárez, and O. Maeso, "Numerical integration scheme for singular integrals based on polar coordinates free from angular quasi-singularities," *Engineering Analysis with Boundary Elements*, Vol.103(C), pp. 126–136, 2005. <https://cdsweb.cern.ch/record/388662>.
- [17] S. Prasad and T. O'Neil, "Waves in a cold pure electron plasma of finite length," *The Physics of Fluids*, Vol.26, pp. 278–281, 1982.
- [18] C. Driscoll, J. Mamlberg, and K. Fine, "Observation of Transport to Thermal Equilibrium in Pure Electron Plasmas," *Physical Review Letters*, Vol.60, pp. 1290–1293, 1987.
- [19] A. Peurrung and J. Fajans, "Non-neutral plasma shapes and edge profiles," *Physics of Fluids B: Plasma Physics 2*, Vol.693, pp. 693–699, 1989.
- [20] S. Prasad and T. O'Neil, "Finite length thermal equilibria of a pure electron plasma," *The Physics of Fluids 22*, Vol.278, pp. 278–281, 1987.
- [21] N. Smirnov, "Table for Estimating the Goodness of Fit of Empirical Distributions.," *Ann. Math. Statist*, Vol.19, pp. 279–281, 1948.
- [22] T. Kirkman, "Statistics to Use," 1996. <http://www.physics.csbsju.edu/stats/KS-test.html>.
- [23] A. Garrett and L. Poladian, "Refined Derivation, Exact Solution and Singular Limits of the Poisson-Boltzmann Equation," *Annals of Physics*, Vol.188, p. 386–435, 1988.
- [24] C. Domine, "2D Particle-In-Cell (PIC) Computer Model for Antimatter Plasma Simulation," *Master Thesis at the University of Manchester, School of Physics and Astronomy*, 2020.
- [25] J. Brackbill, "On energy and momentum conservation in particle-in-cell plasma simulation," *Journal of Computational Physics*, Vol.317, p. 405–427, 2016.
- [26] J. Jackson, *Classical Electrodynamics*. Wiley, 3rd ed., 1999.
- [27] K. Huang, *Statistical Mechanics*. John Wiley and Sons., 2nd ed., 1987.
- [28] R. Davidson, *Physics of non-neutral plasmas*. London: Imperial College Press, 2nd ed., 2001.
- [29] F. Chen, *Introduction to Plasma Physics and Controlled Fusion*. Springer, 3rd ed., 1984.
- [30] G. Andresen *et al.*, "Centrifugal separation and equilibration dynamics in an electron-antiproton plasma," *Physics Review Letter*, Vol.106, 145001, 2011.

This report has been typeset from a TeX/LaTeX file adapted from the MNRAS template (v3.0) by the author.